

UV-Vis Action Spectroscopy of Guanine, 9-Methylguanine, and Guanosine Cation Radicals in the Gas Phase

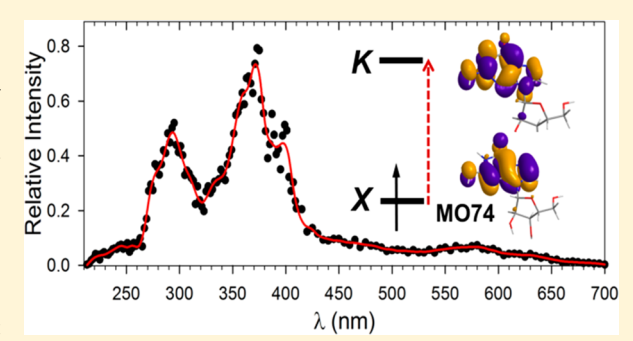
Published as part of The Journal of Physical Chemistry virtual special issue "Pacific Conference on Spectroscopy and Dynamics".

Andy Dang, Yue Liu, and František Tureček*

Department of Chemistry, University of Washington, Bagley Hall, Box 351700, Seattle, Washington 98195-1700, United States

Supporting Information

ABSTRACT: Cation radicals of guanine $(G^{\bullet+})$, 9-methylguanine $(MG^{\bullet+})$, and guanosine $(rG^{\bullet+})$ were generated by dissociative oxidation of gas-phase copper complexes and characterized by UV-vis photodissociation action spectra and ab initio calculations. Comparison of the action spectra of Go+ with the calculated vibronic absorption spectra of several cation radical tautomers showed the best match for the canonical 6-oxo-N-9-H structure (G1°+). The formation of G1°+ was favored by the stability of its precursor Cu^{II} ion complexes in solution and the gas phase. G1^{o+} was the marginally lowest-energy guanine tautomer according to CCSD(T) calculations extrapolated to the complete basis set limit (CBS). A canonical 6-oxo structure (MG1°+) was also assigned to



the 9-methylguanine cation radical on the basis of a match between the action spectrum and the calculated vibronic absorption spectra. MG1°+ was calculated by CCSD(T)/CBS to be marginally less stable than the 6-OH enol tautormer, but its formation was favored by the superior stability of its precursor Cu^{II} ion complexes in solution and the gas phase. Action spectroscopy allowed us to assign the canonical 6-oxo structure (rG1°+) to the gas-phase guanosine cation radicals that were formed as the lowest-energy tautomers. The absorption bands in the action spectra were assigned on the basis of time-dependent density functional theory calculations that were benchmarked on equation-of-motion coupled cluster calculations of Go+.

■ INTRODUCTION

Ionization of nucleic acids with high-energy electrons and photons creates transient cation radicals that undergo fast transformations by electron transfer followed by chemical reactions, resulting in the complex process of DNA damage. Spontaneous electron transfer in randomly ionized nucleic acids is thought to follow a cascade ending at oxidized guanine as the nucleobase of the lowest ionization energy and oxidation potential.²⁻⁸ DNA ionization and electron transfer kinetics have been studied with oligonucleotide models using ingenious methods, 9,10 including identification of reaction products. 11-14 However, spectroscopic characterization of ionized nucleic acids has been hampered by the transient nature of the primary cation radicals. In a seminal study of adenosine and guanosine, Steenken and Jovanovic showed by fast UV-vis spectroscopy that adenosine and guanosine cation radicals produced by pulse radiolysis underwent rapid deprotonation, forming neutral radicals. 6 Guanosine deprotonation following ionization has also been studied by other methods. 17-2 Electron paramagnetic resonance has been the method of choice, although guanosine radicals and cation radicals have been found difficult to distinguish because of spectra similarity.¹⁷ In contrast to ionization in the condensed phase, proton transfer and other side reactions of nucleobase and

nucleoside ions can be controlled in the rarefied gas phase. Nucleobase radicals have been generated by femtosecond electron transfer in the gas phase and characterized by mass spectrometry.²²⁻²⁴ A major advance in the generation of nucleobase cation radicals has been realized by collisioninduced intramolecular electron transfer in transition metal complexes in the gas phase. This method has been developed by Chu, Siu, and co-workers for the generation of peptide cation radicals²⁵ and ingeniously applied by O'Hair,²⁶ Bohme,²⁷ and their co-workers to produce nucleobase and nucleoside cation radicals in the gas phase.²⁸ Ternary complexes of Cu^{II}, nucleobase, and an auxiliary ligand such as 2',2:6',2"-terpyridine (terpy) are produced by electrospray ionization 29,30 as doubly charged ions that are selected by mass and activated by collisions with helium in a mass spectrometer. Collision-induced dissociation (CID) breaks up the complex, oxidizing the nucleobase and forming complementary Cu-(terpy)⁺ and nucleobase cation radical products (Scheme 1) that can be isolated and further characterized by spectroscopy or ion—molecule reactions.^{31–34} In particular, infrared multi-

Received: February 17, 2019 March 20, 2019 Revised: Published: March 26, 2019

Scheme 1. Formation of Gas-Phase Nucleobase Cation Radicals from Cu^{II} Complexes

photon dissociation (IRMPD) spectroscopy^{35,36} has been implemented to determine structures of gas-phase cation radicals of 9-methylguanine, ³⁷ 2'-deoxyguanosine (dG^{•+}), ³⁸ and a guanine–cytosine dimer.³⁹ Recently, UV–vis action spectroscopy⁴⁰ has been applied to the characterization of cation radicals of cytosine⁴¹ and thymine.⁴² Action spectroscopy relies on wavelength-resolved photodissociation of massselected ions whereby the relative intensities of fragment ions are used to reconstruct the absorption bands of the precursor ion. 35,40 Recently, an alternative method of producing cation radicals has been introduced that relies on electron transfer dissociation of doubly charged nucleotide ions⁴³ that has been combined with UV-vis action spectroscopy, as reported for dAA,⁴⁴ chimeric ribonucleotides,⁴⁴ dGG, dGC, and dCG dinucleotides. 45 Here we apply UV-vis action spectroscopy to characterize the cation radicals of guanine $(G^{\bullet+})$, 9methylguanine ($MG^{\bullet+}$), and guanosine ($rG^{\bullet+}$), and we analyze their electronic excitations in the gas phase. We wish to show by experiment and theory that tautomeric forms of guaninerelated cation radicals can be distinguished by UV-vis spectra, and we provide their electronic structure and thermodynamic analysis at a high level of theory.

EXPERIMENTAL SECTION

Materials and Methods. Guanine, 9-methylguanine, guanosine, 2',2:6',2"-terpyridine, and copper nitrate were purchased from Sigma-Aldrich (St. Louis, MO, USA) and used as received. Complexes were made in situ from equimolar concentrations of the components in 50:50 methanol—water and electrosprayed into a Bruker Daltonik (Bremen, Germany) amaZon Speed 3D ion trap mass spectrometer. The ion trap was modified⁴⁶ and equipped with lenses and mirrors to allow irradiation of trapped ions with a laser beam. The beam was generated by an EKSPLA NL301G (Altos Photonics, Bozeman, MT, USA) Nd:YAG laser that was equipped with a PG142C optical parametric oscillator, as described previously for a linear ion trap.⁴⁷ A detailed description of the amaZon ion trap laser UVPD instrument will be published elsewhere.

Calculations. Standard ab initio and density functional theory (DFT) calculations were run with the Gaussian 16 program suite (Revision A01).⁴⁸ A conformation search of

guanosine cation radical structures was performed with Born-Oppenheimer molecular dynamics calculations (BOMD) using the semiemprirical PM6-D3H4 method⁴⁹ run by MOPAC⁵⁰ under the Cuby4 platform. 51 This generated 20 ps trajectories from which several low-energy structures were selected and reoptimized with ωB97X-D⁵² and M06-2X⁵³ hybrid density functional methods using the 6-31+G(dp) basis set. Tautomers of G^{•+}, MG^{•+}, and Cu(terpy) complexes were optimized from initial guess geometries without extensive conformational search. Structures and energies of copper complexes were calculated with CAM-B3LYP, ⁵⁴ ωB97X-D, and M06-2X DFT methods using the 6-311+G(2d,p) basis set. Solvation energies were calculated with self-consistent reaction field methods using the polarizable continuum model⁵⁵ with parameters from Gaussian 16. Additional optimized geometries were obtained with Møller-Plesset calculations, 56 MP2(FULL)/6-31+G-(d,p). The DFT and MP2 geometry optimizations gave very similar structures for individual tautomers of $G^{\bullet+}$, $MG^{\bullet+}$, and dG^{•+} and similar rankings of relative energies. Single-point energies were run on the M06-2X/6-31+G(d,p) optimized geometries with MP2(frozen core) and the aug-cc-pVTZ and aug-cc-pVQZ correlation-consistent basis sets. 57 Another set of single-point energies was obtained with coupled-clusters calculations⁵⁸ with single, double, and disconnected triple excitations, CCSD(T)^{SS} with the aug-cc-pVDZ basis set. Hartree-Fock (HF) and MP2 single-point energies were used to estimate the complete basis set (CBS) limits of correlation energy by fitting with least-squares the formula $E_{corr}(HF) = a +$ Where where X = 2-4 is the ζ split in the aug-cc-pVXZ basis set. 60 Coefficients a, b, and c are given in Table S1 (Supporting Information). Energies extrapolated to the CBS limit were calculated according to the formula E[CCSD(T)/CBS] = $E[HF/aug-cc-pVQZ] + E_{corr}(HF, X \rightarrow \infty) +$ E[CCSD(T)/aug-cc-pVDZ] - E[MP2/aug-cc-pVDZ]. Spin projection 61,62 was used to annihilate higher spin states in HF and MP2 calculations. Vertical excitation energies and oscillator strengths of guanine cation radicals were obtained by equation-of-motion coupled-cluster calculations, EOM-CCSD^{63,64} with the 6-31+G(d,p) basis set. EOM-CCSD energies were calculated for 10 excited states and used to benchmark time-dependent DFT (TD-DFT) calculations 65,66 of several G^{•+} tautomers. On the basis of the benchmarks, we selected UM06-2X/6-31+G(d,p) TD-DFT for calculations of an extensive set of vertical and vibronic transitions in G. $MG^{\bullet+}$, and $rG^{\bullet+}$. To calculate vibronic excitations, we used 300 Boltzmann-ranked ground-state configurations that were generated by the Newton X program⁶⁷ from the harmonic normal modes of each cation radical at 310 K and submitted for TD-DFT calculations. The number of excited states (15-25) was chosen to include excitations with wavelengths down to below 200 nm, covering the experimental wavelength range of 210-700 nm. Unimolecular rate constants were obtained by Rice-Ramsperger-Kassel-Marcus calculations⁶⁸ using the program of Zhu and Hase⁶⁹ that was recompiled for Windows.⁷⁰

■ RESULTS AND DISCUSSION

Cation Radical Generation. Guanine $(G^{\bullet+})$ and 9-methylguanine $(MG^{\bullet+})$ cation radicals were generated in two steps (Scheme 1), which essentially followed the previously reported procedures. ²⁶ In the first step, nucleobase complexes with 2:2',6':2''-terpyridine (terpy) and copper nitrate were made in solution and electrosprayed to produce doubly

charged 2:2',6':2"-terpyridine-Cu-nucleobase complex ions in the gas phase at m/z 223.5 and 230.5 for G and MG, respectively, both for the ⁶³Cu isotope (Figure S1a,b). Following mass selection and collisional activation in the ion trap (CID-MS²), the complexes underwent intramolecular electron transfer that oxidized the nucleobase while dissociating the complex and forming the nucleobase cation radicals at m/z 151 and 165 for $G^{\bullet+}$ and $MG^{\bullet+}$, respectively, as shown in the respective tandem CID-MS³ spectra (Figure S2a,b). Because guanine is sparsely soluble, which limits Cu(terpy) complex formation in aqueous solution, the guanine cation radical was also generated from a Cu(terpy) complex with guanosine (Figure S1c) that upon CID eliminated the sugar moiety to form $[Cu(terpy)G]^{\bullet 2+}$ (m/z 298.5, Figure S1c). This intermediate complex was isolated by mass and subjected to CID-MS³, forming $G^{\bullet+}$. The guanosine cation radical $(rG^{\bullet+})$ was conveniently generated by CID of a doubly charged gasphase Cu complex, $(rG)_3Cu^{2\bullet+}$, m/z 456, according to the reported procedure 27,33 (Figure S3a,b). The gas-phase ions, G^{•+}, MG^{•+}, rG^{•+}, and their Cu-complex precursors, were characterized by accurate mass measurements and CID mass spectra (Table S2).

UV-Vis Photodissociation Action Spectra. Photodissociation of $G^{\bullet+}$ produced three main fragment ions at m/z 110 (loss of N=C=NH radical), m/z 108 (loss of HN= C=O), and m/z 83 (combined loss of N=C-NH and HCN). The mass-resolved fragment ion channels showed different wavelength profiles (Figure 1a-c). The m/z 110 channel (Figure 1a) displayed bands with distinct maxima at 295 and 350 nm and broad, lower-intensity bands at 450-560 nm. The m/z 108 channel (Figure 1b) exhibited bands with maxima at 295 and 380 nm, with a low-intensity tail extending to ca. 500 nm. The m/z 83 channel (Figure 1c) had a major band at 285 nm that coincided with the 295 nm bands of the other fragment ions. In addition, the m/z 83 channel showed broad, low-intensity bands at ca. 350 and 410-550 nm. The total action spectrum, produced by summing the fragment ion intensities, is shown in Figure 1d. The action spectra of Go+ generated by CID-MS³ of the [Cu(terpy)guanosine]^{2•+} complex were virtually identical to those shown in Figure 1a-d and are displayed in Figure S4a-d.

Photodisociation of $MG^{\bullet+}$ generated two main fragment ions at m/z 138 (loss of HCN) and m/z 97 by combined loss of HCN and N=C=NH (Figure 2a). The mass-resolved wavelength profiles showed major bands with maxima at 295 and 350 nm. In addition, the m/z 97 channel showed a very weak band at 450–500 nm. Summing the fragment ion intensities produced the total action spectrum shown in Figure 2h

Photodissociation of $\mathbf{rG}^{\bullet+}$ resulted in the dominant loss of a ribose $C_5H_8O_4$ neutral fragment forming the $\mathbf{G}^{\bullet+}$ ion. The action spectrum displayed two major bands with maxima at 295 and 370 nm and a shoulder at 400 nm extending to 470 nm. There also was a broad, low-intensity band at 530–650 nm with a maximum at 580 nm (Figure 3).

Two features of these UV—vis action spectra are noteworthy. First, one-electron oxidation of the guanine ring has a notable effect on light absorption of the cation radicals. The UV—vis spectrum of neutral guanine in the form of 2′-deoxyguanosine phosphate in aqueous solution has two bands at 255 and 275 nm but no absorption above 300 nm. Absorption spectra of gas-phase guanine have not been recorded because of decomposition, but high-level calculations by Barbatti,

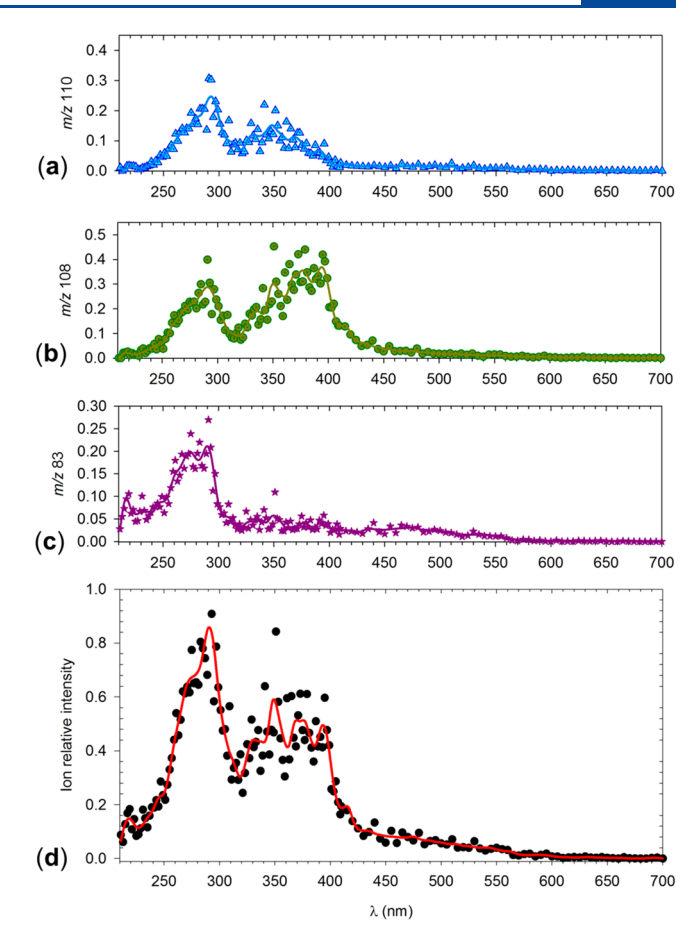


Figure 1. UV–vis photodissociation action spectrum of $G^{\bullet +}$ generated by CID-MS² of the $[Cu(terpy)G]^{2\bullet +}$ complex. (a) m/z 110 photofragment channel; (b) m/z 108 photofragment channel; (c) m/z 83 photofragment channel; (d) sum of photofragment ion intensities. The lines are polynomial fits to the data.

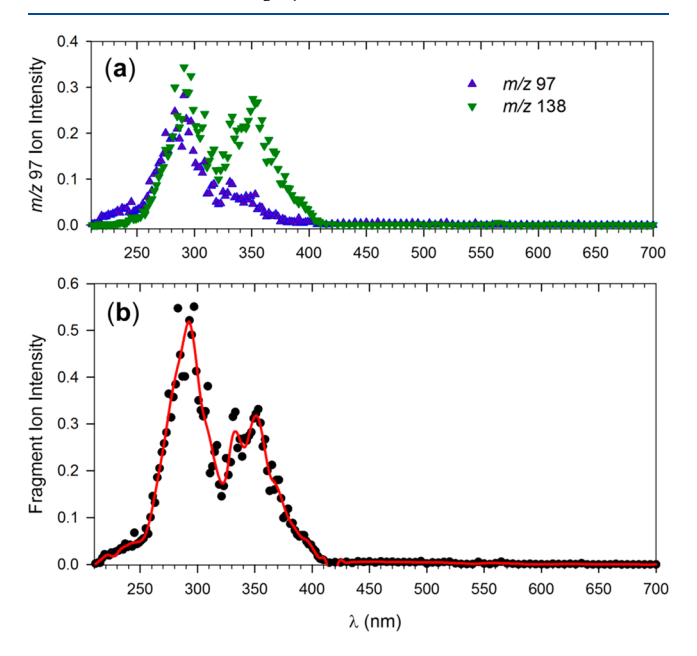


Figure 2. UV—vis photodissociation action spectrum of $MG^{\bullet +}$ generated by CID-MS² of the $[Cu(terpy)MG]^{2\bullet +}$ complex. (a) m/z 97 and 138 photofragment channels; (b) sum of photofragment ion intensities.

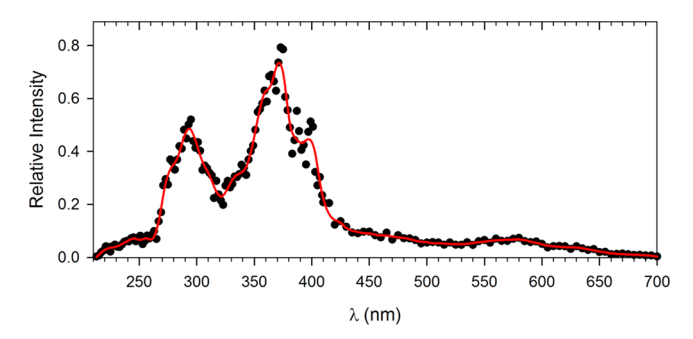


Figure 3. UV-vis photodissociation action spectrum of $rG^{\bullet+}$ generated by CID-MS² of the $[Cu(rG)_3]^{2\bullet+}$ complex.

Lischka, and co-workers indicated guanine absorption bands at 225 and 247 nm. ⁷³ Hence, the bands at $\lambda > 280$ nm that we observed in the UVPD action spectra must be associated with transitions that are typical for the open-shell electronic system of the cation radicals.

Second, it is noteworthy that the fragment ions formed by photodissociation were the same as those from CID (Figure S5a-c). Because ion excitation by collisions in the ion trap proceeds by stepwise vibrational energy deposition in a slowheating mode, the observed CID fragment ions represent products of the lowest-energy dissociations accessed on the ground electronic state. The fact that UVPD and CID of guanine-related cation radicals produced similar fragment ions indicated that the excited electronic states from photoexcitation decayed to a vibrationally excited ground electronic state before dissociation. This is consistent with the wellknown fast internal conversion of nucleobase excited electronic states, which is considered to be crucial for DNA resistance to UV radiation damage. In particular, guanosine $\pi \to \pi^*$ excited states were reported to have 2.5-11 ps lifetimes in aqueous solution, 4 while guanine showed 148–360 fs decay times in the gas phase. Our data indicate that fast excited-state conversion also operates in guanine-related cation radicals in the gas phase.

Cation Radical Structures and Relative Energies. To aid the interpretation of the UV-vis action spectra, we carried out extensive calculations that were aimed at three goals. First, we investigated the energetics of guanine and 9-methylguanine Cu(terpy) complexes in water and the gas phase. This was motivated by the mode of cation radical formation in our experiments that involved Cu complexes as precursor ions that were produced from solution and transferred to the gas phase by electrospray ionization. Second, we investigated the relative energies of gas-phase cation radicals of guanine (G°+), 9methylguanine (MG*+), 2'-deoxyguanosine (dG*+), and guanosine (rG*+) to establish their stabilities and potential for isomerization upon CID. We note that the energetics of MG*+ and dG*+ have been addressed by O'Hair and coworkers using DFT calculations.^{37,38} We now extend the energy calculations to the CCSD(T)/CBS level of theory, which is the gold standard for thermochemical calculations. Finally, we use TD-DFT calculations to produce excitation energies and oscillator strengths for several low-energy G^{•+}, MG^{•+}, and rG^{•+} tautomers to be compared with the UV-vis action spectra. The TD-DFT-calculated spectra were benchmarked on the equation-of-motion CCSD calculations of lowenergy **G**^{•+} tautomers.

Guanine Structures and Energies. Structures and relative free energies of aqueous quaternary complexes of guanine tautomers with [Cu(terpy)NO₃]*+ were obtained by three DFT methods (Table S3). According to these calculations, guanine preferred binding to [Cu(terpy)NO₃]*+ as a canonical 6-oxo-N-9-H tautomer (complexes CuG1*+ and CuG3*+) or as an 6-oxo-N-7-H tautomer (CuG2*+), forming low free-energy complexes (Figure 4). Complexes of other guanine 6-oxo tautomers (CuG4*+-CuG8*+, Figure S6, Table S3) were less stable. Binding to [Cu(terpy)NO₃]*+ of the guanine 6-OH-N-9-H tautomer CuG4*+ was ca. 30 kJ mol⁻¹ weaker than that for the N-9-H tautomer (Figure S6, Table S3). DFT calculations of solvated neutral guanine also indicated the 6-oxo-N-9-H and 6-oxo-N-7-H tautomers as the preferred low-free energy structures that are expected to be

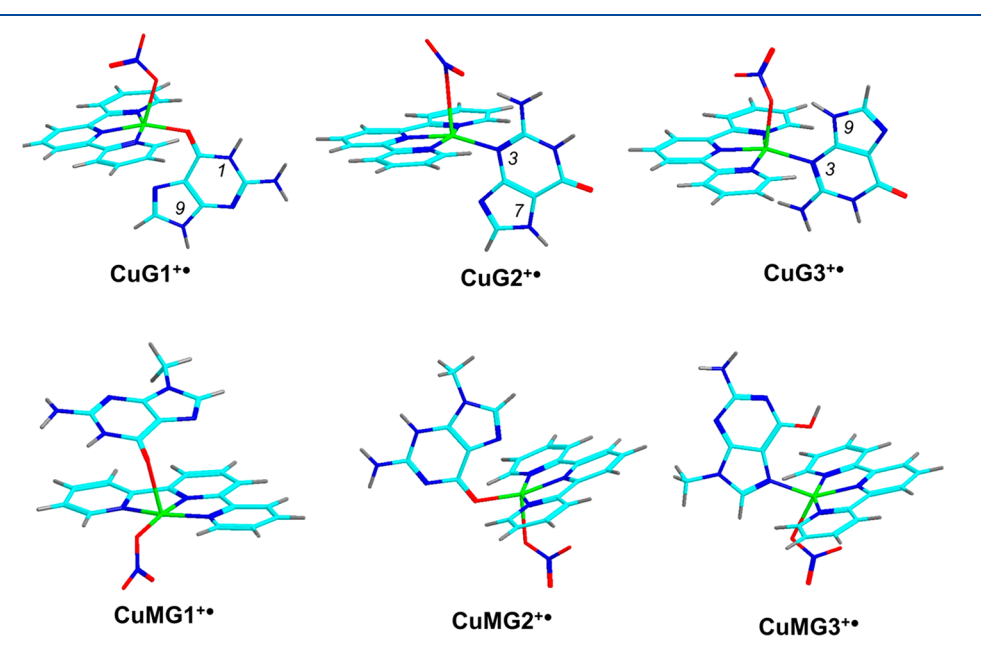


Figure 4. M06-2X/6-311+G(2d,p) optimized structures of $[Cu(terpy)(NO_3)G]^{\bullet+}$ and $[Cu(terpy)(NO_3)MG]^{\bullet+}$ complexes. Atom color coding is as follows: light green = Cu, cyan = C, blue = N, red = O, gray = H.

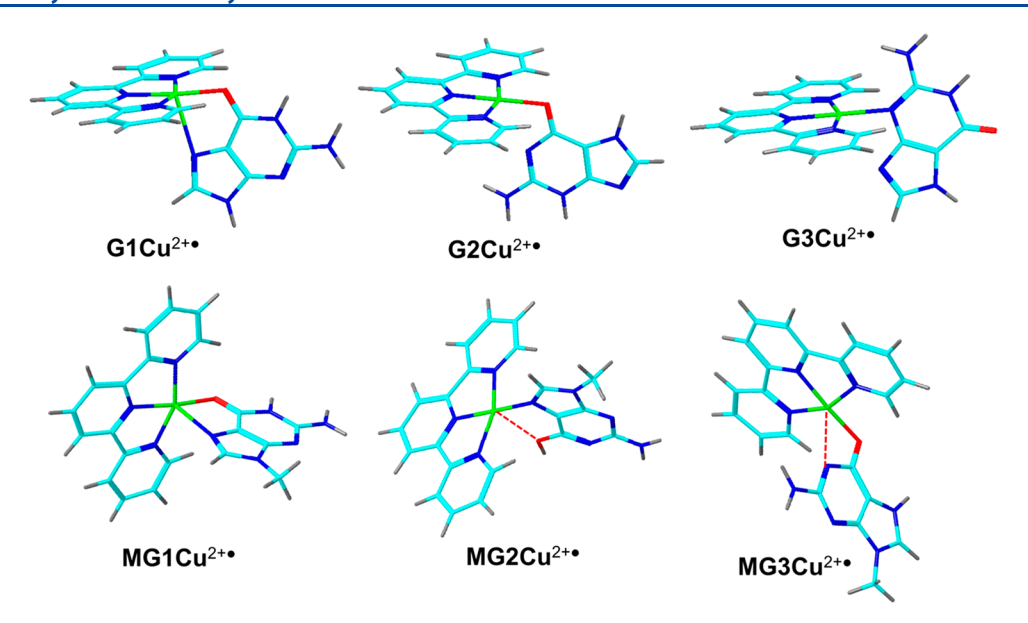


Figure 5. M06-2X/6-311+G(2d,p) optimized structures of low-energy gas-phase $[Cu(terpy)G]^{2\bullet+}$ and $[Cu(terpy)MG]^{2\bullet+}$ complexes. Atom color coding is as in Figure 4.

Table 1. Relative Energies of [Guanine] + Isomers a,b

ion or reaction	$M06-2X^c$	ω B97X-D ^d	$PMP2^{c}$	$CCSD(T)^{c,e}$	CCSD(T) ^f
	6-311++G(2d,p)		aug-cc-pVTZ		CBS
G1 ^{•+}	0.0	0.0	0.0	0.0	0.0 (0.0) ^g
$G2^{\bullet+}$	0.8	8.7	0.0	3.5	2.8 (2.9)
G3°+	7.4	15	3.7	9.1	8.6 (9.2)
$G4^{\bullet+}$	8.7	9.0	7.2	6.2	5.6 (5.6)
G5 ^{•+}	18	27	15	18	18 (18)
G6 ^{•+}	69	68	64		
$\mathbf{G7}^{ullet+}$	76	72	66		
$G8^{\bullet+}$	66	73	54		
$G1^{\bullet+} \rightarrow m/z \ 108 + HNCO$	361	354	336	342	349
$G1^{\bullet+} \rightarrow m/z \ 110 + HNC=N^{\bullet}$	310	325	294	283	271

"In kJ mol⁻¹. ^bIncluding B3LYP/6-31+G(d,p) zero-point energies and referring to 0 K unless stated otherwise. ^cSingle-point energies on M06-2X/6-31+G(d,p) optimized geometries. ^dSingle-point energies on ω B97X-D/6-31+G(d,p) optimized geometries. ^eExtrapolated single-point energies: $E[CCSD(T)/aug\text{-cc-pVTZ}] \approx E[CCSD(T)/aug\text{-cc-pVDZ}] + E[PMP2/aug\text{-cc-pVTZ}] - E[PMP2/aug\text{-cc-pVDZ}]$. ^fSingle-point energies extrapolated to the CBS. ^gRelative free energies at 310 K.

predominantly represented in aqueous solution to form Cu complexes. According to the calculations, dissociation of the lowest free-energy solvated quaternary complex $\text{CuG1}^{\bullet +}$ to $[\text{Cu(terpy)NO}_3]^{\bullet +}(\text{aq}) + \text{G(aq)}$ and $[\text{Cu}^{\text{II}}(\text{terpy)G}]^{2\bullet +}(\text{aq}) + \text{NO}_3^-(\text{aq})$ was endothermic, $\Delta G_{298,\text{aq}} = 25$ and 34 kJ mol⁻¹, respectively (Table S3), indicating micromolar formation constants in water and justifying our representation of the solution complexes shown in Scheme 1. We note that weak peaks of the quaternary complexes were present in the electrospray spectra (Figure S1a-c).

After transfer to the gas phase and counterion separation, the ternary $[Cu(terpy)G]^{2\bullet+}$ complexes favored the structure with an N-3 and O-6 dicoordinated canonical guanine $(G1Cu^{2\bullet+}, Figure 5)$. The second-lowest-energy complex $(G2Cu^{2\bullet+})$ included the N-3-H, N-7-H guanine tautomer coordinated to Cu by O-6 (Table S4). The other complexes $(G3Cu^{2\bullet+}-G7Cu^{2\bullet+})$, including that of the 6-OH enol form of guanine, were disfavored by ca. 40 kJ mol⁻¹ (Figure S7, Table S4).

Relative energies of gas-phase $G^{\bullet +}$ tautomers were calculated at several levels of theory and are displayed in Table 1. According to the calculations, the gas-phase canonical structure $G1^{\bullet +}$ with the 6-oxo, N-1-H, and N-9-H arrangement was the lowest-energy tautomer. Because this tautomer also formed low-energy solvated quaternary and gas-phase ternary complexes with Cu(terpy), we considered it the best candidate for the gas-phase ion formed in the ion trap. The *syn-* and *anti-*6-OH tautomers $G2^{\bullet +}$ and $G3^{\bullet +}$ were 3-9 kJ mol $^{-1}$ less stable

than G1°+ when based on the CCSD(T)/CBS energies. These tautomers did not form low-energy Cu complexes, and therefore, their potential presence in the gas phase could only be because of isomerization upon CID. The N-7-H tautomer (G4°+) was within 5.6 kJ mol⁻¹ of G1°+ (Table 1) and formed a low-energy quaternary Cu complex in solution. Thus, G4°+ was considered a plausible candidate for the gasphase ions. We note that the relative energies of G1°+-G4°+ obtained from M06-2X calculations were in a very good agreement with the benchmark CCSD(T)/CBS data and thus appeared to be reliable for estimates of relative energies of larger ions where CCSD(T) calculations may not be feasible. Several other tautomeric combinations were investigated (G5°+-G8°+) but were found to be much less stable than G1^{•+}.

9-Methylquanine Structures and Energies. Aqueous quaternary complexes of MG with [Cu(terpy)NO₃]*+ showed preference for structure CuMG1°+ (Figure 4, Table S5) in which MG was in the canonical 6-oxo, N-1-H form that was coordinated to Cu^{II} by the 6-oxo group. Complexes of the N-3-H (CuMG2°+), 6-OH (CuMG3°+), and N-7-H (CuMG4°+) tautomers were substantially less stable and were not expected to be present in solution at equilibrium. The gas-phase MG complexes also largely favored the canonical 6-oxo form MG1Cu^{2•+} (Table S6) in which MG was coordinated to Cu^{II} by O-6 and N-7 (Figure 5). MG1Cu²⁰⁺ can be formed from the lowest-energy quaternary complex CuMG1°+ by ion separation upon electrospray. Hence, coordination to Cu^{II}(terpy) in both solution and the gas-phase complexes favored the canonical MG tautomer over isomers.

The gas-phase MG^{•+} tautomers showed three structures of very similar energy (Table 2). The syn-6-OH tautomer MG2^{•+} was the lowest-energy structure, which was within 1 kJ mol⁻¹ of the canonical 6-oxo tautomer MG1°+ according to CCSD(T)/CBS calculations. The anti-6-OH rotamer (MG3°+) was within 3-6 kJ mol⁻¹ of MG1°+, whereas the 6-oxo-N-7-H tautomer (MG4°+) was 58 kJ mol⁻¹ less stable (Table 2). We note that only MG1°+ can be formed without rearrangement from the low-energy Cu complexes CuMG1°+ and MG1Cu^{2•+} that were expected to dominate in solution and the gas phase. The other low-energy MG*+ tautomers can be produced only by CID-triggered proton transfer isomerizations.

Guanosine Structures and Energies. Similar to $G^{\bullet+}$, the guanosine cation radicals favored the canonical tautomer rG1°+ as the lowest-energy structure. The syn- and anti-6-OH enol forms (rG2°+ and rG3°+, respectively) had higher relative energies at all levels of theory that we investigated. Further, 6oxo tautomers with the N-7-H (rG4°+) and N-3-H (rG5°+) arrangements had substantially higher relative energies (Table 3). We found a similar ranking of relative energies for the four lowest-energy tautomers of [deoxyguanosine] •+ (dG1 •+ -

Table 2. Relative Energies of [9-Methylguanine] •+ Isomers^{a,b}

ion or reaction		ω B97X-D ^d		$CCSD(T)^{c,e}$	CCSD(T) ^f CBS
	6-311++G(2d,p)		aug	-cc-pVTZ	СВЗ
$MG1^{\bullet +}$	0.0	0.0	0.0	0.0	$0.0 (0.0)^g$
MG2 ^{•+}	-0.4	9.3	-3.9	-3.7	-2.2(-1.0)
MG3°+	5.5	17	-0.7	2.0	1.8 (3.0)
MG4 ^{•+}	66	56	57	58	
MG5°+	111	115			
MG6°+	85	85	96		

^aIn kJ mol⁻¹. ^bIncluding B3LYP/6-31+G(d,p) zero-point energies and referring to 0 K unless stated otherwise. ^cSingle-point energies on M06-2X/6-31+G(d,p) optimized geometries. ^dSingle-point energies on ωB97X-D/6-31+G(d,p) optimized geometries. Extrapolated single-point energies: $E[CCSD(T)/aug\text{-cc-pVTZ})] \approx E[CCSD(T)/aug\text{-cc-pVTZ}]$ aug-cc-pVDZ)] + E[PMP2/aug-cc-pVTZ)] - E[PMP2/aug-ccpVDZ)]. fSingle-point energies extrapolated to the CBS. gRelative free energies at 310 K.

dG5°+) that were analyzed at the same level of theory for comparison (Table S7, Figure S8).

We investigated the dissociation energy of rG1°+ that was of interest with regard to the CID and UVPD spectra that indicated facile loss of the ribose moiety. G1°+-forming dissociation was found to essentially follow the route elucidated by O'Hair et al. for [deoxyguanosine] •+ 38 This consisted of cleavage of the N-9-C-1' bond to reach a complex of the guanyl radical with the ribose cation ($\mathbf{rG6}^{\bullet+}$). In contrast to O'Hair et al., we found the electron distribution in the intermediate complex of guanosine to involve a ribose C-1' cation and a guanine radical. This was obvious from the analysis of spin densities that pointed to ~100% of unpaired electron density to be in the guanine ring (Scheme 2). Also, the planar geometry at the ribose C-1' in rG6°+ was highly indicative of a carbocation. The further reaction course involved a transition state (TS(rG)^{•+}) undergoing simultaneous closure of the 1,5'-anhydroribose ring and proton transfer onto N-9 and forming a low-energy complex (rG7°+, Scheme 2). In accord with the previous analysis of O'Hair et al., $TS(rG)^{\bullet+}$ at 131 kJ mol⁻¹ relative to $rG1^{\bullet+}$ was also the highest energy point on the potential energy surface for rG1°+ dissociation.³⁸ The threshold energy for the separation of G1^{•+} and 1,5-anhydroribose was calculated to be 96 kJ mol⁻¹ relative to rG1°+ at the CCSD(T)/CBS level of theory, and this final step of dissociation in rG7°+ was presumed to be continuously endothermic. Compared to the CCSD(T)/CBS energetics of the analogous dissociation of [deoxyguanosine] •+ (Table S7), the dissociation of rG1°+ required a slightly higher energy transition state and intermediates. This was consistent with the formation of a ribose C-1' cation in $rG6^{\bullet+}$ and $TS(rG^{\bullet+})$, which was destabilized in the presence of the electronwithdrawing 2'-OH group. Interestingly, attempts at exploring participation by the 2'-OH group in the cleavage of the C-1'-N-9 bond in rG1°+ did not result in the formation of stable intermediates as the system collapsed to rG6°+ upon gradient geometry optimization.

With regard to the photodissociation experiments, we used the $TS(rG^{\bullet+})$ energy to calculate the unimolecular rate constants for dissociation of rG1°+ when driven by the absorbed photon energy. The results (Figure S9) indicated that absorption of a single photon of λ < 650 nm can trigger dissociation on the 50 ms experimental time scale.

Table 3. Relative Energies of [Guanosine] * Isomers a,b

ion or reaction	M06-2X ^c	ω B97X-D ^d	$PMP2^{c}$	$CCSD(T)^{c,e}$	CCSD(T) ^f
	6-311++G(2d,p)		aug-	cc-pVTZ	CBS
rG1*+	0.0	0.0	0.0	0.0	0.0 (0.0) ^g
rG2•+	7.9	17	8.2	9.9	8.8 (9.8)
rG3°+	12	21	11	14	13 (14)
rG4 ^{•+}	53	50			
rG5°+	76	73			
$TS(rG)^{\bullet+}$	138	133	138	132	131
rG6°+	132	129	134	130	126
rG7 ^{•+}	38	35	35	33	31 (23)
$G1^{\bullet+} + C_5H_8O_4^h$	103	103	111	105	96 (48)
2.123 rG1		rG2+•	Y	2.073	rG4**
1.782 2.256 rG5+•	rG6*	1.642	rG7**	2.203	2.359

^aIn kJ mol⁻¹. ^bIncluding B3LYP/6-31+G(d,p) zero-point energies and referring to 0 K unless stated otherwise. ^cSingle-point energies on M06-2X/6-31+G(d,p) optimized geometries. ^dSingle-point energies on ω B97X-D/6-31+G(d,p) optimized geometries. ^eExtrapolated single-point energies: $E[CCSD(T)/aug\text{-cc-pVTZ})] \approx E[CCSD(T)/aug\text{-cc-pVDZ})] + E[PMP2/aug\text{-cc-pVTZ})] − E[PMP2/aug\text{-cc-pVDZ})]$. ^fSingle-point energies extrapolated to the CBS. ^gRelative free energies at 310 K. ^hFor the 1,5-anhydroribose neutral fragment.

Furthermore, the $\mathbf{rG1}^{\bullet+}$ lifetime dropped to a few ns at excitation energies achieved by absorption of photons of $\lambda < 250$ nm. This indicated that $\mathbf{rG1}^{\bullet+}$ can dissociate within a 3–6 ns laser pulse, and the resulting [guanosine] $^{\bullet+}$ can absorb another photon from the same pulse to drive its consecutive dissociation.

Excited Electronic States and Comparison of Theoretical Absorption and Experimental Action Spectra. To interpret the UV—vis action spectra, we carried out calculations of excited-state energies and oscillator strengths for multiple tautomers of $\mathbf{G}^{\bullet+}$, $\mathbf{MG}^{\bullet+}$, and $\mathbf{rG}^{\bullet+}$ that allowed us to obtain theoretical absorption spectra. The calculations were augmented by including excitations from multiple Boltzmann-populated vibrational states to produce vibronic absorption spectra at 310 K. The excited-state calculations were carried out with TD-DFT M06-2X that was benchmarked to EOM-CCSD with the 6-31+G(d,p) basis set.

Guanine Cation Radicals. Starting with G1°+, the calculated absorption spectrum (Figure 6b) showed six major lines that were broadened to overlapping bands with maxima at 230, 270, 340, 360, and 440 nm and extended as a weak broad shoulder to 530 nm. Another very weak line appeared at 610 nm. The excitation lines from the benchmarking EOM-CCSD calculations (blue lines in Figure

6b) were generally blue-shifted relative to those from TD-DFT M06-2X, but both sets showed correlating wavelengths and oscillator strengths. We note that a previous benchmarking study of radical excitations⁶⁶ found that increasing the basis set in EOM-CCSD calculations resulted in 0.1-0.2 eV red shifts of the excitation energies. Thus, through error cancellation, the current TD-DFT M06-2X calculations were expected to achieve a reasonably accurate description of electronic excitations in the nucleobase radicals. The calculated absorption spectra of the syn- and anti-OH rotamers G2°+ and G3°+ were very similar and are here represented by the calculated excitation lines and vibronic spectrum of G2°+ (Figure 6c). The TD-DFT lines appeared at 214, 222, 238, 276, 345, 403, and 505 nm that were broadened into bands with maxima at 223, 262, 275, 345, 400, and 495 nm in the vibronic spectrum. The EOM-CCSD excitation lines showed a close correlation and a blue shift relative to the M06-2X ones. A different absorption spectrum was calculated for G4°+ (Figure 6d), which showed major TD-DFT lines at 213, 251, 282, 322, 390, and 493 nm, in close correlation with EOM-CCSD. Vibronic broadening resulted in bands with maxima at 220, 280, 390, and 490 nm for G4^{o+}.

When comparing the calculated vibronic spectra of $G1^{\bullet+}$ – $G4^{\bullet+}$ with the action spectrum (Figure 6a), we found the

Scheme 2. Intermediates and Transition State for Dissociations of [Guanosine] + Isomer rG1 + a

^aItalics show the calculated atomic spin densities in rG6^{•+}.

closest match for G1°+ (Figure 6b). The match was based on (1) the low intensity in the action spectrum of the 230 nm band, (2) the shape and position of the main band at 290 nm, and (3) the composite band at 340-380 nm. The 420-550 nm tail in the action spectrum also had a matching feature in the vibronic spectrum of G1°+ (Figure 6b), although this region was also represented in the vibronic spectra of G2°+ and G4°+. We note that small (estimated <5%) fractions of G2°+ and G4°+ could not be excluded on the basis of the spectra alone. However, attempts at fitting the action spectrum by a Boltzmann-weighed mixture of vibronic spectra of G1°+-G4°+, when based on the CCSD(T)/CBS free energies (Table 1), resulted in a poor match. Hence, we conclude that the canonical guanine cation radical structure G1°+ was represented in the gas phase, originating from the most stable quaternary Cu(terpy)NO₃ complex in solution via a ternary Cu(terpy) complex produced by electrospray. The formation of G1°+ from the guanosine complex, as evidenced by the matching action spectrum (Figure S4), was consistent with the proposed dissociation mechanism.

The electronic excitations in G1°+ for several excited states are summarized in Table S8 and illustrated with the relevant molecular orbitals (Figure 7). The first (A) excited state of $\Delta E_{\rm exc}$ = 2.03 eV corresponded to a dipole-disallowed transition from the highest π_{xy} orbital (MO38) to the singly occupied molecular orbital (MO39, SOMO), which was of π_z type. MO38 was a combination of n-type orbitals at N-3, N-7, and O-6. This transition had a very low oscillator strength (0.0002) and appeared in neither the calculated absorption nor the action spectrum. The second (B) excited state, corresponding to the transition $\pi_{xy}({\rm MO36}) \rightarrow {\rm SOMO}$ of $\Delta E_{\rm exc}$ = 2.55 eV,

was likewise dipole-forbidden and was not observed. The longest-wavelength band that appeared in the spectrum was due to the C excited state, arising from the dipole-allowed $\pi_z(\text{MO35}) \to \text{SOMO}$ excitation of $\Delta E_{\text{exc}} = 2.88$ eV. Further dipole-allowed excitations to the SOMO accounted for the D ($\pi_z(\text{MO37})$, $\Delta E_{\text{exc}} = 3.23$ eV) and E states ($\pi_z(\text{MO34})$, $\Delta E_{\text{exc}} = 3.71$ eV). The most intense transition at 258 nm of $\Delta E_{\text{exc}} = 4.80$ eV involved electron excitation from the SOMO to the virtual orbital space, chiefly involving the $\pi_z(\text{MO40})$ and $\pi_z(\text{MO41})$ orbitals (Figure 7).

Methylguanine Cation Radicals. The calculated absorption spectra of 9-methyl guanine tautomers displayed different bands (Figure 8b-e) to be compared with the action spectrum (Figure 8a). The canonical isomer MG1°+ had five major excitation lines at 223, 258, 261, 333, and 379 and a very weak line at 494 nm that gave rise to vibronically broadened bands in the spectrum (Figure 8b). The absorption spectrum of MG1°+ showed an excellent match with the action spectrum of [9-methylguanine] •+ (Figure 8a). In contrast, the absorption spectra of low-energy tautomers MG2°+ and MG3°+ (Figure 8c,d) were distinctly different in that they had different patterns of dominant bands at 220-230 and 400 nm that were much less evident in the action spectrum. A less stable isomer (MG6°+, Figure 8e) had an intense band at 276 nm that was analogous to the 290 nm band in the action spectrum. However, MG6°+ further displayed a composite band at 220 nm and a broad band at 595 nm that were not pronouncedly represented in the action spectrum. Our assignment of the action spectrum belonging to the canonical isomer MG1°+ is in perfect agreement with the previous conclusion by O'Hair and co-workers that they made on the basis of an infrared action

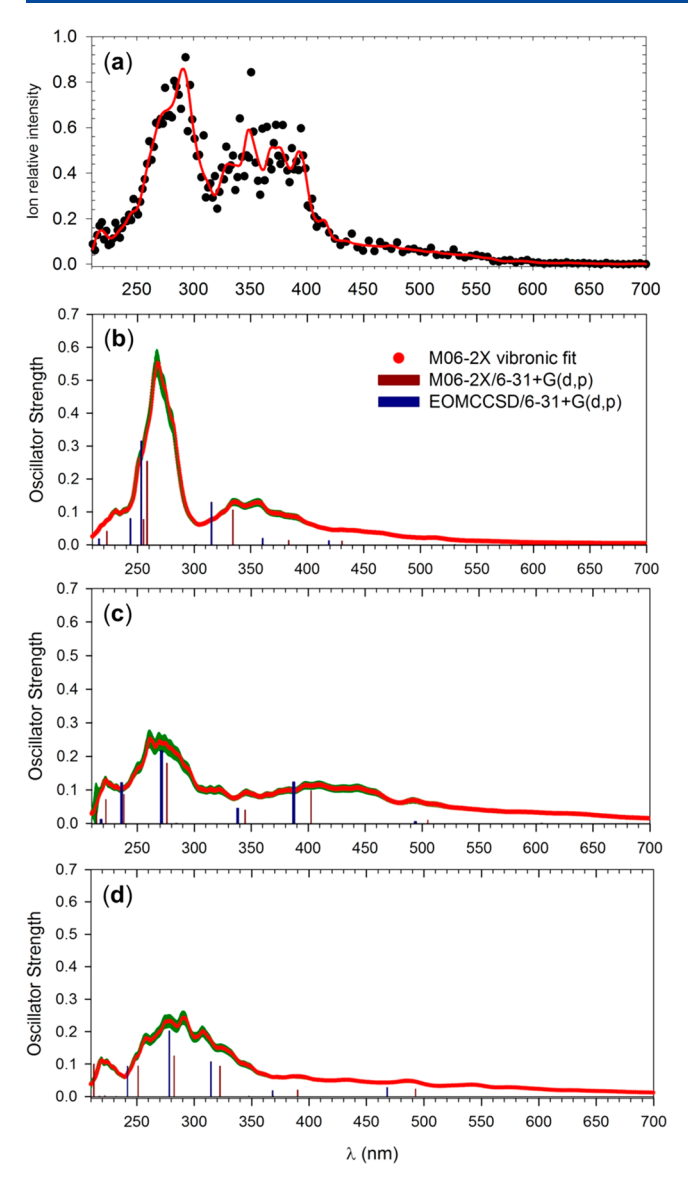


Figure 6. (a) Action spectrum of [guanine] $^{\bullet+}$; M06-2X/6-31+G(d,p) TD-DFT line, vibronic, and EOM-CCSD line spectra fits for (b) G1 $^{\bullet+}$, (c) G2 $^{\bullet+}$, and (d) G4 $^{\bullet+}$. Green vertical lines indicate error bars in the vibronic spectra calculations.

spectrum.³⁷ The electronic excitations in MG1°+ occurred on a manifold of excited states that closely resembled that for G1°+. The transitions are summarized in Table S9 and visualized in Figure S10. It is worth noting that MG1°+ is not the lowest free-energy isomer among the [9-methylguanine] + ions (Table 2). However, the canonical structure was highly energetically preferred in the ion precursors that were the Cu^{II}(terpy) complexes in solution and the gas phase. Under equilibrium conditions in solution, the calculated relative free energies (Table S5) suggested CuMG1°+ to represent >99% of the isomer population. Hence, the dominant formation of MG1°+ in the gas-phase ion population can be explained by selection of the canonical MG1 tautomer when binding in the Cu^{II} complex. At the same time, the absence of low-energy isomers MG2°+ and MG3°+ among the gas-phase ion population indicated that the Cu^{II}-coordinated nucleobase ligand did not undergo proton transfer isomerization in the course of electron transfer oxidation upon CID.

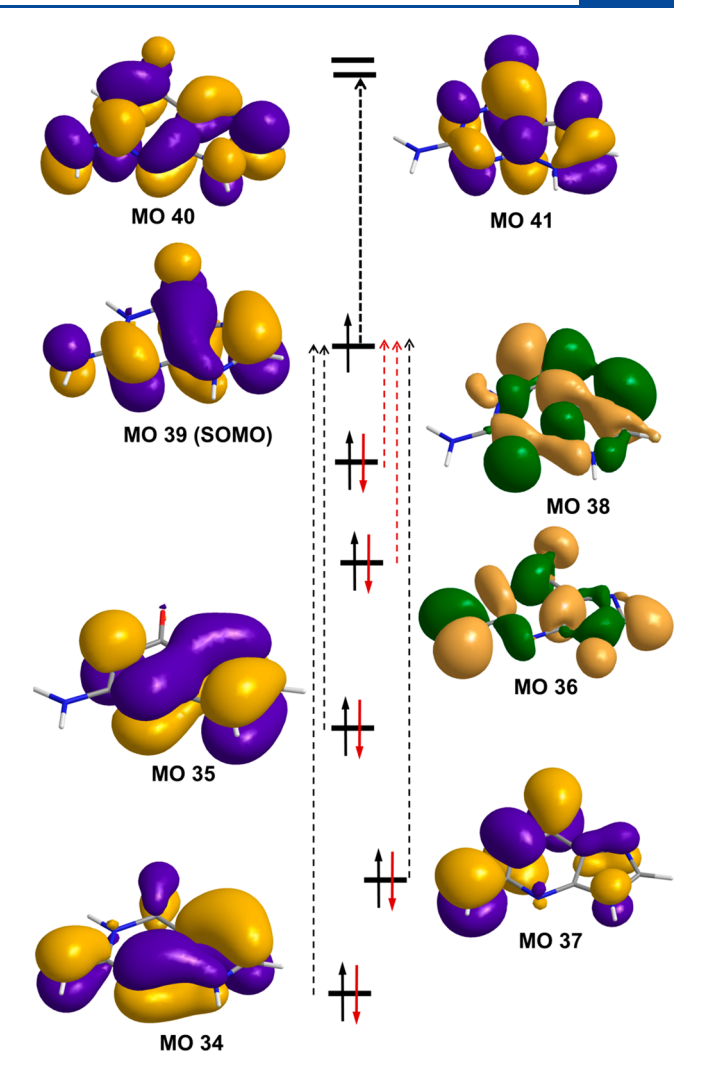


Figure 7. Molecular orbitals of ground and excited electronic states in $G1^{\bullet+}$ from M06-2X/6-31+G(d,p) calculations. Black broken-line arrows indicate dipole-allowed electronic excitations, and red arrows are for dipole-disallowed ones. Refer to Table S8 for the excited-state assignment, excitation energies, and oscillator strength.

Guanosine Cation Radicals. The calculated absorption spectra of guanosine tautomers differed in displaying several distinct bands (Figure 9b-d). The canonical isomer rG1°+ had two prominent absorptions at 261 and 264 nm that were accompanied by weaker lines at 221, 332, 371, and 507 nm (Figure 9b). The syn- and anti-6-OH isomers showed stronger lines at 222 and 245 nm and prominent lines at 282-284 nm. Further distinction was indicated by four lines in the 340-450 nm region and weak lines at 560-563 nm (Figure 9c,d). In addition, the vibronic spectra showed distinctly different transitions from higher vibrational states, which is particularly illustrated by broad bands with maxima at 400-420 nm for rG2°+ and rG3°+. This broad band was not represented in the action spectrum of [guanosine] + (Figure 9a), indicating that rG2*+ and rG3*+ were not substantially populated among the gas-phase ions. The absorption spectrum of rG1°+ provided matching wavelengths for the band maxima with those in the action spectrum. However, the band relative intensities differed. In particular, the band group at 250 and 290 nm was weaker than the 370 nm band in the action spectrum, contrasting the corresponding band intensities in the calculated vibronic spectrum. We propose an explanation of this

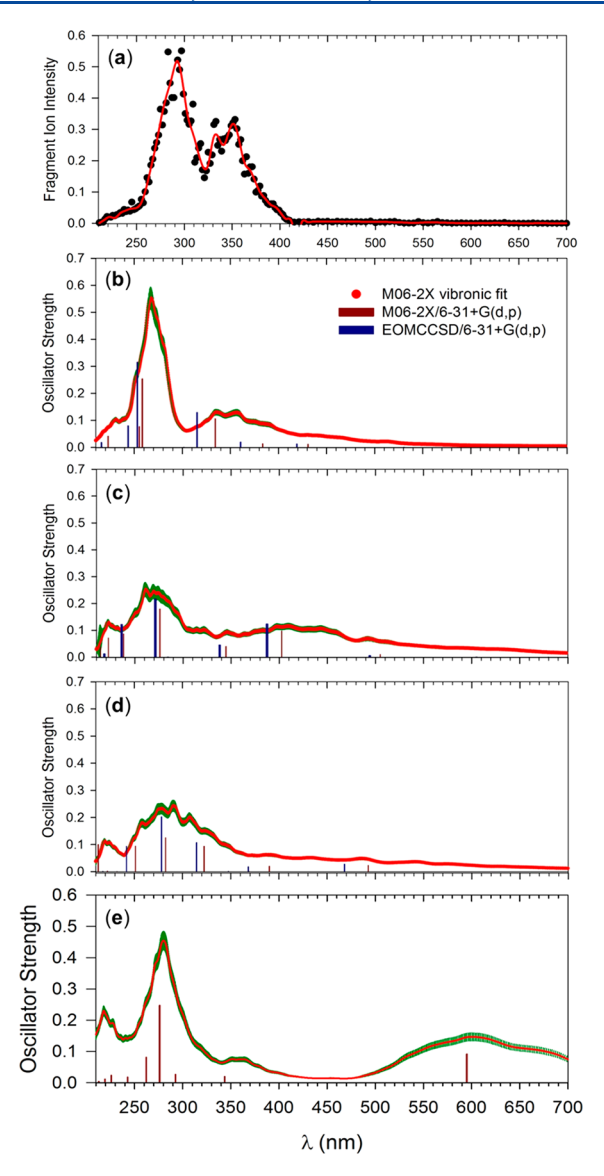


Figure 8. (a) Action spectrum of [9-methylguanine]^{•+}; M06-2X/6-31+G(d,p) TD-DFT line, vibronic, and EOM-CCSD line spectra fits for (b) MG1^{•+}, (c) MG2^{•+}, (d) MG3^{•+}, and (e) MG6^{•+}. Green vertical lines indicate error bars in the vibronic spectra calculations.

discrepancy on the basis of the kinetics for the main photodissociation channel, which was loss of 1,5-anhydroribose (Scheme 2). The dissociation can be accomplished at the 50 ms time scale by single-photon absorption at wavelengths of up to ca. 650 nm. At photon wavelengths below ca. 300 nm, the excited ion lifetime dropped below 5 ns, producing vibrationally excited products. On the basis of energy balance, the excitation energy was estimated to be $E_{\rm exc} = E(h\nu)$ - $E(\text{diss}) = 400-96 = 304 \text{ kJ mol}^{-1} \text{ at } 300 \text{ nm that was}$ partitioned between the G1°+ and 1,5-anhydroribose products. Assuming that the excess energy was partitioned according to the fragments' heat capacities at the equivalent temperature of 940 K,⁷⁶ the G1^{•+} ion received an energy of 163 kJ mol⁻¹ from photodissociation at 300 nm. Note that this internal excitation would be insufficient to drive the dissociation of G1°+ that had a calculated energy threshold at $271~\mathrm{kJ~mol^{-1}}$ (Table 1). However, because of the extremely fast photofragmentation, the nascent G1°+ ion can absorb a photon from the same laser pulse and undergo consecutive dissociation. The nearly

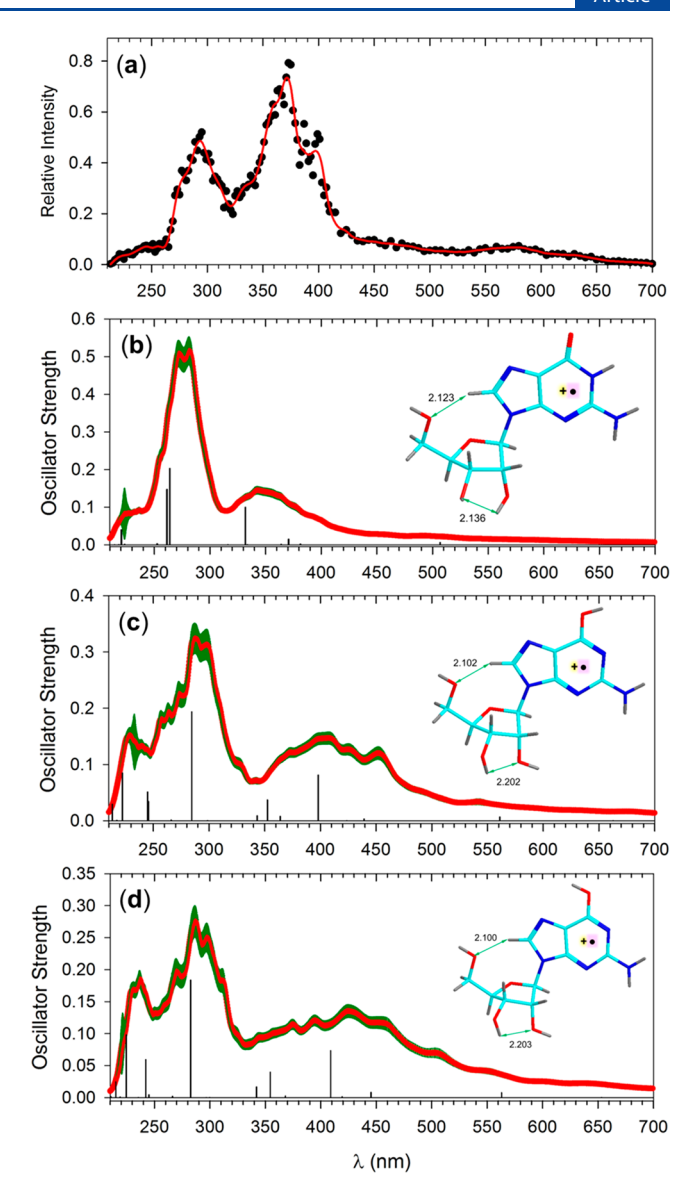


Figure 9. (a) Action spectrum of [guanosine]*; M06-2X/6-31+G(d,p) TD-DFT line and vibronic spectra fits for (b) rG1*+, (c) rG2*+, and (d) rG3*+.

matching bands at 220 and 280–290 nm in the action spectra of $\mathbf{rG1}^{\bullet+}$ and $\mathbf{G1}^{\bullet+}$ would allow absorption of consecutive photons. The dissociation of $\mathbf{G1}^{\bullet+}$ depleted the primary photofragment ion intensity and resulted in reduced intensity of the short-wavelength bands in the action spectrum of $\mathbf{rG1}^{\bullet+}$. Note that the photodissociation of $\mathbf{rG1}^{\bullet+}$ on the laser pulse 5 ns time scale rapidly dropped at $\lambda > 350$ nm, indicating that the main 370 nm band in the action spectrum should not be affected. On the basis of this analysis, we assign the action spectrum of [guanosine] $^{\bullet+}$ to the lowest-energy isomer $\mathbf{rG1}^{\bullet+}$. We note that our assignment for [guanosine] $^{\bullet+}$ is consistent with the conclusion of O'Hair et al. for [2'-deoxyguanosine] $^{\bullet+}$ that was made on the basis of infrared action spectra. ³⁸

The electron transitions leading to excited states in $\mathbf{rG1}^{\bullet+}$ (Table S10) were analogous to those in $\mathbf{MG1}^{\bullet+}$. The ribose moiety was not involved in the dominant excitations that involved the $\pi_z \to \mathrm{SOMO}(\mathrm{MO74})$ and $\mathrm{SOMO} \to \pi_z^*$ type transitions forming excited states $H(\lambda_{\mathrm{max}} = 332 \ \mathrm{nm}), K(\lambda_{\mathrm{max}} = 264 \ \mathrm{nm}), L(\lambda_{\mathrm{max}} = 261 \ \mathrm{nm}), \text{ and } O(\lambda_{\mathrm{max}} = 221 \ \mathrm{nm})$ (Table

S10). Charge transfer transitions involving ribose ionization were apparent in excited states $E(\lambda_{max} = 371 \text{ nm})$ and $M(\lambda_{max} = 253 \text{ nm})$. The pertinent molecular orbitals in $\mathbf{rG1}^{\bullet+}$ are visualized in Figure S11.

CONCLUSIONS

Action spectroscopy in the gas phase allowed us to obtain mass-resolved UV-vis spectra of canonical forms of guanine, 9-methylguanine, and guanosine cation radicals that were free of interferences from proton transfer and radical reaction products. The spectra showed common bands at 350-400 nm that were assigned to internal $\pi_z \to SOMO$ electron excitations within the β -orbital manifold and were found to be characteristic of the open-shell electronic system. The two lowest excited states of guanine, 9-methylguanine, and guanosine cation radicals were calculated to be dark states of near-zero oscillator strength in the visible region of the spectrum. The UV-vis spectra of the canonical cation radical isomers were distinctly different from those calculated for tautomers and can be used for isomer identification. The common band features found in the action spectra may represent benchmarks for the identification of transient guanine cation radicals produced by DNA ionization.

ASSOCIATED CONTENT

S Supporting Information

The Supporting Information is available free of charge on the ACS Publications website at DOI: 10.1021/acs.jpca.9b01542.

Complete ref 48, correlation energies, accurate masses, relative energies and optimized structures of Cu complexes, electron transitions, electrospray and CID mass spectra, UV-vis action spectrum, RRKM kinetic plots of ion lifetimes, and molecular orbital diagrams of excited states (PDF)

AUTHOR INFORMATION

Corresponding Author

*E-mail: turecek@chem.washington.edu.

ORCID

František Tureček: 0000-0001-7321-7858

Notes

The authors declare no competing financial interest.

ACKNOWLEDGMENTS

Financial support from the Chemistry Division of the National Science Foundation (Grants CHE-1661815 for experiments and CHE-1624430 for calculations) is gratefully acknowledged. F.T. acknowledges the Klaus and Mary Ann Saegebarth Endowment for general support.

■ REFERENCES

- (1) Khanna, K. K.; Jackson, S. P. DNA Double-Strand Breaks: Signaling, Repair and the Cancer Connection. *Nat. Genet.* **2001**, *27*, 247–254.
- (2) Hush, N. S.; Cheung, A. S. Ionization Potentials and Donor Properties of Nucleic Acid Bases and Related Compounds. *Chem. Phys. Lett.* **1975**, *34*, 11–13.
- (3) Sugiyama, H.; Saito, I. Theoretical Studies of GG-Specific Photocleavage of DNA via Electron Transfer: Significant Lowering of Ionization Potential and 5'-Localization of HOMO of Stacked GG Bases in B-Form DNA. J. Am. Chem. Soc. 1996, 118, 7063–7068.

- (4) Jovanovic, S. V.; Simic, M. G. One-Electron Redox Potentials of Purines and Pyrimidines. *J. Phys. Chem.* **1986**, *90*, 974–978.
- (5) Psciuk, B. T.; Lord, R. L.; Munk, B. H.; Schlegel, H. B. Theoretical Determination of One-Electron Oxidation Potentials for Nucleic Acid Bases. *J. Chem. Theory Comput.* **2012**, *8*, 5107–5123.
- (6) Langmaier, J.; Samec, Z.; Samcova, E.; Hobza, P.; Reha, D. Origin of Difference between One-Electron Redox Potentials of Guanosine and Guanine: Electrochemical and Quantum Chemical Study. *J. Phys. Chem. B* **2004**, *108*, 15896–15899.
- (7) Bi, S.; Liu, B.; Fan, F.-R. F.; Bard, A. J. Electrochemical Studies of Guanosine in DMF and Detection of Its Radical Cation in a Scanning Electrochemical Microscopy Nanogap Experiment. *J. Am. Chem. Soc.* **2005**, 127, 3690–3691.
- (8) Crespo-Hernandez, C. E.; Close, D. M.; Gorb, L.; Leszczynski, J. Determination of Redox Potentials for the Watson-Crick Base Pairs, DNA Nucleosides, and Relevant Nucleoside Analogs. *J. Phys. Chem. B* **2007**, *111*, 5386–5395.
- (9) O'Neill, M. A.; Barton, J. K. Sequence-Dependent DNA Dynamics: The Regulator of DNA-mediated Charge Transport. In Charge Transfer in DNA: From Mechanism to Application; Wagenknecht, H.-A., Ed.; Wiley-VCH: Weinheim, 2005; pp 27–77.
- (10) Kim, H.; Budzinski, E. E.; Box, H. C. The Radiation-Induced Oxidation and Reduction of Guanine: Electron Spin Resonance-Electron Nuclear Double Resonance Studies of Irradiated Guanosine Cyclic Monophosphate. *J. Chem. Phys.* **1989**, *90*, 1448–1451.
- (11) Meggers, E.; Dussy, A.; Schafer, T.; Giese, B. Electron Transfer in DNA from Guanine and 8-Oxoguanine to a Radical Cation of the Carbohydrate Backbone. *Chem. Eur. J.* **2000**, *6*, 485–492.
- (12) Shukla, L. I.; Pazdro, R.; Huang, J.; DeVreugd, C.; Becker, D.; Sevilla, M. D. The Formation of DNA Sugar Radicals from Photoexcitation of Guanine Cation Radicals. *Radiat. Res.* **2004**, *161*, 582–590
- (13) Onyemauwa, F. O.; Schuster, G. B. The Reaction of Water with Guanosine Radical Cation in DNA. *Photochem. Photobiol.* **2006**, 82, 729–732.
- (14) Khanduri, D.; Collins, S.; Kumar, A.; Adhikary, A.; Sevilla, M. D. Formation of Sugar Radicals in RNA Model Systems and Oligomers via Excitation of Guanine Cation Radical. *J. Phys. Chem. B* **2008**, *112*, 2168–2178.
- (15) Shafirovich, V.; Geacintov, N. E. Spectroscopic Investigation of Charge Transfer in DNA. In *Charge Transfer in DNA: From Mechanism to Application*; Wagenknecht, H.-A., Ed.; Wiley-VCH: Weinheim, 2005; pp 175–196.
- (16) Steenken, S.; Jovanovic, S. V. How Easily Oxidizable Is DNA? One-Electron Reduction Potentials of Adenosine and Guanosine Radicals in Aqueous Solution. *J. Am. Chem. Soc.* **1997**, *119*, 617–618.
- (17) Bachler, V.; Hildenbrand, K. EPR-Detection of the Guanosyl Radical Cation in Aqueous Solution. Quantum Chemically Supported Assignment of Nitrogen and Proton Hyperfine Couplings. *Radiat. Phys. Chem.* **1992**, 40, 59–68.
- (18) Kobayashi, K.; Tagawa, S. Direct Observation of Guanine Radical Cation Deprotonation in Duplex DNA Using Pulse Radiolysis. *J. Am. Chem. Soc.* **2003**, *125*, 10213–10218.
- (19) Morozova, O. B.; Saprygina, N. N.; Fedorova, O. S.; Yurkovskaya, A. V. Deprotonation of Transient Guanosyl Cation Radical Catalyzed by Buffer in Aqueous Solution: TR-CIDNP Study. *Appl. Magn. Reson.* **2011**, *41*, 239–250.
- (20) Morozova, O. B.; Fishman, N. N.; Yurkovskaya, A. V. Indirect NMR Detection of Transient Guanosyl Radical Protonation in Neutral Aqueous Solution. *Phys. Chem. Chem. Phys.* **2017**, *19*, 21262–21266.
- (21) Choi, J.; Yang, C.; Fujitsuka, M.; Tojo, S.; Ihee, H.; Majima, T. Proton Transfer of Guanine Radical Cations Studied by Time-Resolved Resonance Raman Spectroscopy Combined with Pulse Radiolysis. *J. Phys. Chem. Lett.* **2015**, *6*, 5045–5050.
- (22) Wolken, J. K.; Syrstad, E. A.; Vivekananda, S.; Tureček, F. Uracil Radicals in the Gas Phase. Specific Generation and Energetics. *J. Am. Chem. Soc.* **2001**, *123*, 5804–5805.

- (23) Syrstad, E. A.; Vivekananda, S.; Tureček, F. Direct Observation of a Hydrogen Atom Adduct to C-5 in Uracil. A Neutralization-Reionization Mass Spectrometric and ab initio Study. *J. Phys. Chem. A* **2001**, *105*, 8339–8351.
- (24) Yao, C.; Cuadrado-Peinado, M.; Polášek, M.; Tureček, F. Specific Generation of 1-Methylcytosine Radicals in the Gas-Phase. *Angew. Chem., Int. Ed.* **2005**, *44*, 6708–6711.
- (25) Chu, I. K.; Rodriquez, C. F.; Lau, T.-C.; Hopkinson, A. C.; Siu, K. W. M. Molecular Radical Cations of Oligopeptides. *J. Phys. Chem.* B 2000, 104, 3393–3397.
- (26) Wee, S.; O'Hair, R. A. J.; McFadyen, W. D. Can Radical Cations of the Constituents of Nucleic Acids Be Formed in the Gas Phase Using Ternary Transition Metal Complexes? *Rapid Commun. Mass Spectrom.* **2005**, *19*, 1797–1805.
- (27) Cheng, P.; Bohme, D. K. Gas-Phase Formation of Radical Cations of Monomers and Dimers of Guanosine by Collision-Induced Dissociation of Cu(II)-Guanosine Complexes. *J. Phys. Chem. B* **2007**, *111*, 11075–11082.
- (28) Zhang, S.; Xu, L.; Dong, J.; Cheng, P.; Zhou, Z.; Fu, J. Collision-Induced Dissociation of Singly and Doubly Charged CuII-Cytidine Complexes in the Gas Phase: An Experimental and Computational Study. *RSC Adv.* **2012**, *2*, 2568–2575.
- (29) Gatlin, C. L.; Tureček, F.; Vaisar, T. Copper(II) Amino Acid Complexes in the Gas Phase. *J. Am. Chem. Soc.* **1995**, *117*, 3637–3638.
- (30) Tureček, F. Copper-Biomolecule Complexes in the Gas Phase. The Ternary Way. *Mass Spectrom. Rev.* **2007**, *26*, 563–582.
- (31) Sun, Y.; Zhou, W.; Moe, M. M.; Liu, J. Reactions of Water with Radical Cations of Guanine, 9-Methylguanine, 2'-Deoxyguanosine and Guanosine: Keto-Enol Isomerization, C8-Hydroxylation, and Effects of N9-Substitution. *Phys. Chem. Chem. Phys.* **2018**, 20, 27510–27522.
- (32) Liguori, A.; Napoli, A.; Sindona, G. Electron Transfer vs. Proton Transfer within Radical-Cation Clusters of Guanosine and Deoxyguanosine with Substituted Naphthalenes and Sinapinic Acid. *J. Am. Soc. Mass Spectrom.* **2001**, *12*, 176–179.
- (33) Feketeova, L.; Yuriev, E.; Orbell, J. D.; Khairallah, G. N.; O'Hair, R. A. J. Gas-Phase Formation and Reactions of Radical Cations of Guanosine, Deoxyguanosine and Their Homodimers and Heterodimers. *Int. J. Mass Spectrom.* **2011**, *304*, 74–82.
- (34) Cheng, P.; Li, Y.; Li, S.; Zhang, M.; Zhou, Z. Collision-Induced Dissociation (CID) of Guanine Radical Cation in the Gas Phase: An Experimental and Computational Study. *Phys. Chem. Chem. Phys.* **2010**, *12*, 4667–4677.
- (35) Polfer, N. C., Dugourd, P., Eds. Laser Photodissociation and Spectroscopy of Mass Separated Biomolecular Ions. *Lecture Notes in Chemistry*; Springer: Cham, 2013; Vol. 83, pp 13–20.
- (36) Dunbar, R. C. Photodissociation of Trapped Ions. Int. J. Mass Spectrom. 2000, 200, 571-589.
- (37) Feketeova, L.; Khairallah, G. N.; Chan, B.; Steinmetz, V.; Maitre, P.; Radom, L.; O'Hair, R. A. J. Gas-Phase Infrared Spectrum and Acidity of the Radical Cation of 9-Methylguanine. *Chem. Commun.* **2013**, *49*, 7343–7345.
- (38) Feketeova, L.; Chan, B.; Khairallah, G. N.; Steinmetz, V.; Maitre, P.; Radom, L.; O'Hair, R. A. J. Gas-Phase Structure and Reactivity of the Keto Tautomer of the Deoxyguanosine Radical Cation. *Phys. Chem. Chem. Phys.* **2015**, *17*, 25837–25844.
- (39) Feketeova, L.; Chan, B.; Khairallah, G. N.; Steinmetz, V.; Maitre, P.; Radom, L.; O'Hair, R. A. J. Watson-Crick Base Pair Radical Cation as a Model for Oxidative Damage in DNA. *J. Phys. Chem. Lett.* **2017**, *8*, 3159–3165.
- (40) Antoine, R.; Dugourd, P. UV-Visible Activation of Biomolecular Ions. (Laser Photodissociation and Spectroscopy of Mass-Separated Biomolecular Ions). Lect. Notes Chem. 2013, 83, 93–116.
- (41) Lesslie, M.; Lawler, J. T.; Dang, A.; Korn, J. A.; Bím, D.; Steinmetz, V.; Maitre, P.; Tureček, F.; Ryzhov, V. Cytosine Radical Cation: A Gas-Phase Study Combining IRMPD Spectroscopy, UV-PD Spectroscopy, Ion—Molecule Reactions, and Theoretical Calculations. *ChemPhysChem* **2017**, *18*, 1293—1301.

- (42) Dang, A.; Nguyen, H. T. H.; Ruiz, H.; Piacentino, E.; Ryzhov, V.; Tureček, F. Experimental Evidence for Non-Canonical Thymine Cation Radicals in the Gas Phase. *J. Phys. Chem. B* **2018**, *122*, 86–97.
- (43) Hari, Y.; Leumann, C. J.; Schurch, S. What Hinders Electron Transfer Dissociation (ETD) of DNA Cations? *J. Am. Soc. Mass Spectrom.* **2017**, 28, 2677–2685.
- (44) Korn, J. A.; Urban, J.; Dang, A.; Nguyen, H. T. H.; Turecek, F. UV-Vis Action Spectroscopy Reveals a Conformational Collapse in Hydrogen-Rich Dinucleotide Cation Radicals. *J. Phys. Chem. Lett.* **2017**, *8*, 4100–4107.
- (45) Liu, Y.; Korn, J. A.; Dang, A.; Turecek, F. Hydrogen-Rich Cation Radicals of DNA Dinucleotides. Generation and Structure Elucidation by UV-Vis Action Spectroscopy. *J. Phys. Chem. B* **2018**, 122, 9665–9680.
- (46) Martens, J.; Berden, G.; Gebhardt, C. R.; Oomens, J. Infrared ion spectroscopy in a modified quadrupole ion trap mass spectrometer at the FELIX free electron laser laboratory. *Rev. Sci. Instrum.* **2016**, *87*, 103108/1–103108/8.
- (47) Shaffer, C. J.; Pepin, R.; Tureček, F. Combining UV Photodissociation Action Spectroscopy with Electron Transfer Dissociation for Structure Analysis of Gas-Phase Peptide Cation-Radicals. J. Mass Spectrom. 2015, 50, 1438–1442.
- (48) Frisch, M. J.; Trucks, G. W.; Schlegel, H. B.; Scuseria, G. E.; Robb, M. A.; Cheeseman, J. R.; Scalmani, G.; Barone, V.; Petersson, G. A.; Nakatsuji, H.; et al. *Gaussian 16*, revision A01; Gaussian, Inc.: Wallingford, CT, 2016.
- (49) Řezáč, J.; Fanfrlík, J.; Salahub, D.; Hobza, P. Semi-Empirical Quantum Chemical PM6Method Augmented by Dispersion and H Bonding Correction Terms Reliably Describes Various Types of Noncovalent Complexes. J. Chem. Theory Comput. 2009, 5, 1749—1760.
- (50) Stewart, J. J. P. *MOPAC 16*; Stewart Computational Chemistry: Colorado Springs, CO, 2016.
- (51) Řezáč, J. Cuby: An Integrative Framework for Computational Chemistry. *J. Comput. Chem.* **2016**, *37*, 1230–1237.
- (52) Chai, J. D.; Head-Gordon, M. Long-Range Corrected Hybrid Density Functionals with Damped Atom-Atom Dispersion Corrections. *Phys. Chem. Chem. Phys.* **2008**, *10*, 6615–6620.
- (53) Zhao, Y.; Truhlar, D. G. The M06 Suite of Density Functionals for Main Group Thermochemistry, Thermochemical Kinetics, Noncovalent Interactions, Excited States, and Transition Elements: Two New Functionals and Systematic Testing of Four M06-Class Functionals and 12 Other Functionals. *Theor. Chem. Acc.* 2008, 120, 215–241.
- (54) Yanai, T.; Tew, D. P.; Handy, N. C. A New Hybrid Exchange-Correlation Functional Using the Coulomb-Attenuating Method (CAM-B3LYP). *Chem. Phys. Lett.* **2004**, 393, 51–57.
- (55) Tomasi, J.; Mennucci, B.; Cammi, R. Quantum Mechanical Continuum Solvation Models. *Chem. Rev.* **2005**, *105*, 2999–3093.
- (56) Møller, C.; Plesset, M. S. A Note on an Approximation Treatment for Many-Electron Systems. *Phys. Rev.* **1934**, *46*, 618–622.
- (57) Dunning, T. H., Jr. Gaussian Basis Sets for Use in Correlated Molecular Calculations. I. The Atoms Boron Through Neon and Hydrogen. *J. Chem. Phys.* **1989**, *90*, 1007–1023.
- (58) Čížek, J. On the Use of the Cluster Expansion and the Technique of Diagrams in Calculations of Correlation Effects in Atoms and Molecules. *Adv. Chem. Phys.* **2007**, *14*, 35–89.
- (59) Purvis, G. D., III; Bartlett, R. J. A. Full Coupled-Cluster Singles and Doubles Model the Inclusion of Disconnected Triples. *J. Chem. Phys.* **1982**, *76*, 1910–1918.
- (60) Halkier, A.; Helgaker, T.; Jørgensen, P.; Klopper, W.; Koch, H.; Olsen, J.; Wilson, A. K. Basis Set Convergence in Correlated Calculations on Ne, N₂, and H₂O. *Chem. Phys. Lett.* **1998**, 286, 243–252.
- (61) Schlegel, H. B. Potential Energy Curves Using Unrestricted M? ller-Plesset Perturbation Theory with Spin Annihilation. *J. Chem. Phys.* **1986**, *84*, 4530.

- (62) Mayer, I. Spin-Projected UHF Method. IV. Comparison of Potential Curves Given by Different One-Electron Methods. *Int. J. Quantum Chem.* **1978**, *14*, 29–38.
- (63) Sekino, H.; Bartlett, R. J. A Linear Response, Coupled-Cluster Theory for Excitation Energy. *Int. J. Quantum Chem.* **1984**, 26, 255–265.
- (64) Comeau, D. C.; Bartlett, R. J. The Equation-of-Motion Coupled- Cluster Method. Applications to Open- and Closed-Shell Reference States. *Chem. Phys. Lett.* **1993**, 207, 414–423.
- (65) Furche, F.; Ahlrichs, A. Adiabatic Time-Dependent Density Functional Methods for Excited State Properties. *J. Chem. Phys.* **2002**, 117, 7433–7447.
- (66) Turecek, F. Benchmarking Electronic Excitation Energies and Transitions in Peptide Radicals. *J. Phys. Chem. A* **2015**, *119*, 10101–10111
- (67) Barbatti, M.; Ruckenbauer, M.; Plasser, F.; Pittner, J.; Granucci, G.; Persico, M.; Lischka, H. Newton-X: A Surface-Hopping Program for Nonadiabatic Molecular Dynamics. *Wiley Interdisciplinary Reviews: Comput. Mol. Sci.* **2014**, *4*, 26–33.
- (68) Gilbert, R. G.; Smith, S. C. Theory of Unimolecular and Recombination Reactions; Blackwell Scientific Publications: Oxford, 1990; pp 52–132.
- (69) Zhu, L.; Hase, W. L. Quantum Chemistry Program Exchange, Program No. QCPE 644; Indiana University: Bloomington, IN, 1994. (70) Frank, A. J.; Sadílek, M.; Ferrier, J. G.; Turecek, F. Sulfur Oxoacids and Radicals in the Gas Phase. A Variable-Time Neutralization-Photoexcitation- Reionization Mass Spectrometric and Ab initio/RRKM Study. J. Am. Chem. Soc. 1997, 119, 12343—12353.
- (71) Petroselli, G.; Dantola, M. L.; Cabrerizo, F. M.; Capparelli, A. L.; Lorente, C.; Oliveros, E.; Thomas, A. H. Oxidation of 2'-Deoxyguanosine 5'-Monophosphate Photoinduced by Pterin: Type I versus Type II Mechanism. *J. Am. Chem. Soc.* **2008**, *130*, 3001–3011.
- (72) Clark, L. B.; Peschel, G. G.; Tinoco, I. Vapor Spectra and Heats of Vaporization of Some Purine and Pyrimidine Bases. *J. Phys. Chem.* **1965**, *69*, 3615–3618.
- (73) Barbatti, M.; Aquino, A. J. A.; Lischka, H. The UV Absorption of Nucleobases: Semi-Classical ab Initio Spectra Simulations. *Phys. Chem. Chem. Phys.* **2010**, *12*, 4959–4967.
- (74) Kang, H.; Lee, K. T.; Jung, B.; Ko, Y. J.; Kim, S. K. Intrinsic Lifetimes of the Excited State of DNA and RNA Bases. *J. Am. Chem. Soc.* **2002**, *124*, 12958–12959.
- (75) Canuel, C.; Mons, M.; Piuzzi, F.; Tardivel, B.; Dimicoli, I.; Elhanine, M. Excited States Dynamics of DNA and RNA Bases: Characterization of a Stepwise Deactivation Pathway in the Gas Phase. J. Chem. Phys. 2005, 122, 074316.
- (76) Pepin, R.; Tureček, F. Kinetic Ion Thermometers for Electron Transfer Dissociation. *J. Phys. Chem. B* **2015**, *119*, 2818–2826.